Atmospheric
Chemistry
and Physics
Discussions

Discussion Paper

Secondary organic aerosol formation from biomass burning intermediates: phenol and methoxyphenols

L. D. Yee[1], K. E. Kautzman[2,*], C. L. Loza[2], K. A. Schilling[2], M. M. Coggon[2], P. S. Chhabra[2,], M. N. Chan[1,***], A. W. H. Chan[2,****], S. P. Hersey[1], J. D. Crounse[3], P. O. Wennberg[1,3], R. C. Flagan[2,1], and J. H. Seinfeld[2,1]**

[1]Division of Engineering and Applied Science, California Institute of Technology, Pasadena, CA, USA
[2]Division of Chemistry and Chemical Engineering, California Institute of Technology, Pasadena, CA, USA
[3]Division of Geological and Planetary Sciences, California Institute of Technology, Pasadena, CA, USA
[*]now at: Department of Chemistry, Towson University, Towson, MD, USA
[**]now at: Aerodyne Research Inc., Billerica MA, USA
[***]now at: Chemical Sciences Division, Lawrence Berkeley National Laboratory, Berkeley, CA, USA
[****]now at: Department of Environmental Science, Policy and Management, University of California, Berkeley, Berkeley, CA, USA

3485

Abstract

The formation of secondary organic aerosol from oxidation of phenol, guaiacol (2-methoxyphenol), and syringol (2,6-dimethoxyphenol), major components of biomass burning, is described. Photooxidation experiments were conducted in the Caltech laboratory chambers under low-NO$_x$ (<10 ppb) conditions using H$_2$O$_2$ as the OH source. Secondary organic aerosol (SOA) yields (ratio of mass of SOA formed to mass of primary organic reacted) greater than 25 % are observed. Aerosol growth is rapid and linear with the primary organic conversion, consistent with the formation of essentially non-volatile products. Gas- and aerosol-phase oxidation products from the guaiacol system provide insight into the chemical mechanisms responsible for SOA formation. Syringol SOA yields are lower than those of phenol and guaiacol, likely due to novel methoxy group chemistry that leads to early fragmentation in the gas-phase photooxidation. Atomic oxygen to carbon (O:C) ratios calculated from high-resolution-time-of-flight Aerodyne Aerosol Mass Spectrometer (HR-ToF-AMS) measurements of the SOA in all three systems are ∼0.9, which represent among the highest such ratios achieved in laboratory chamber experiments and are similar to that of aged atmospheric organic aerosol. The global contribution of SOA from intermediate volatility and semivolatile organic compounds has been shown to be substantial (Pye and Seinfeld, 2010). An approach to representing SOA formation from biomass burning emissions in atmospheric models could involve one or more surrogate species for which aerosol formation under well-controlled conditions has been quantified. The present work provides data for such an approach.

1   Introduction

Biomass burning is a major source of atmospheric organic aerosol (OA), with contributions from both anthropogenic (biofuel, deforestation, etc.) as well as natural sources such as wildfires. Aerosol produced from biomass burning has been estimated to ac-

count for 90 % of all primary organic carbon emitted globally from combustion sources (Ito and Penner, 2005). Bond et al. (2004) estimated global annual emissions of carbonaceous aerosol due to combustion as 8.0 Tg for black carbon (BC) and 33.9 Tg organic carbon (OC). Biofuel and open burning were estimated by these authors to account, respectively, for 20 % and 42 % of BC, and 19 % and 74 %, of OC. The amount and composition of organic aerosol formed from these sources vary widely based on combustion conditions and fuel type. Measured wood smoke emissions from fireplaces, for example, depend strongly on the type of fuel consumed and can vary in magnitude by a factor of five for different fuel sources and sampling techniques (Fine et al., 2001). Particulate matter from biomass burning, including wildfires, residential wood burning, and deforestation is also of major concern for visibility, climate change and health effects (Naeher et al., 2007).

The pyrolysis of lignin, the second most abundant polymer on Earth comprising the secondary cell wall of plants, produces phenols. Hawthorne et al. (1989) showed that phenols and methoxyphenols account for a significant fraction of particulate matter derived from wood smoke, constituting 21 % and 45 % by mass of total aerosol, respectively. Emission rates for methoxyphenol species from biomass burning have been estimated to range from 420–900 mg kg^{-1} fuel (Hawthorne et al., 1989, 1992; Schauer et al., 2001). In addition to the significant emission factors of these compounds, guaiacol, which is emitted from both hard and soft wood combustion, and syringol, which is emitted primarily from soft woods, have been proposed as aerosol markers for wood combustion as well as biomarkers to determine human exposure levels (Dills et al., 2001; Simpson and Naeher, 2010).

Here we investigate the aerosol-forming potential of phenol and two of the most abundant methoxyphenol species, guaiacol and syringol (Table 1). Both guaiacol and phenol are intermediate volatility organic compounds; syringol has a vapor pressure 100 times less than those of phenol and guaiacol. The molecular structures are shown in Table 1 along with vapor pressures and reaction rate constants with OH. Here we determine the fractional yield of secondary organic aerosol (SOA) from photooxidation

of phenol, guaiacol, and syringol by OH in laboratory chamber studies under low-NO$_x$ (< 10 ppb) conditions. In addition, we present analyses of the gas- and particle-phase constituents in guaiacol photooxidation to elucidate the chemical mechanism involved in guaiacol SOA formation. We qualitatively compare the chemistry of the test compounds to explore why syringol results in lower SOA yield compared to phenol and guaiacol. A further motivation for this work is the potential use of phenol, guaiacol, and syringol as compounds to represent biomass burning emissions in atmospheric models of organic aerosol formation. SOA products identified in the laboratory studies may also serve as markers for biomass burning in ambient aerosols.

2 Experimental section

2.1 Chamber experiments

All experiments were carried out in the Caltech dual 28 m^3 Teflon chambers. Details of the facilities have been described previously (Cocker et al., 2001; Keywood et al., 2004). Before each experiment, the chambers were flushed with dried purified air for > 24 h, until the particle number concentration was < 100 cm^{-3} and the volume concentration was < 0.1 µm^3 cm^{-3}. In all yield experiments, ammonium sulfate seed aerosol was used to promote condensation of low volatility oxidation products. The seed aerosol was generated by atomization of a 0.015 M aqueous ammonium sulfate solution. Following atomization, the size distribution of the seed particles peaked at ~ 56 nm with an average number concentration of ~ 2700 cm^{-3}, and a total seed volume concentration of 10–15 µm cm^{-3} was achieved. The hydrocarbon was introduced into the chamber by injecting a known volume of pure hydrocarbon into a glass bulb and flowing purified air over the hydrocarbon at 5 L min^{-1} until the hydrocarbon had fully vaporized.

For these low-NO$_x$ experiments, hydrogen peroxide (H$_2$O$_2$) was used as the OH precursor. Prior to atomization of the ammonium sulfate seed, H$_2$O$_2$ was introduced

by flowing 5 L min^{-1} of purified air through a glass trap containing 280 µL of a 50 % aqueous H$_2$O$_2$ solution. The glass trap was submerged in a warm water bath maintained at 35–38 °C. This resulted in an approximate concentration of 4 ppm H$_2$O$_2$ in the chamber.

The aerosol number concentration and size distribution were measured by a differential mobility analyzer (DMA, TSI model 3081) coupled with a condensation nuclei counter (TSI, CNC-3760). After allowing all concentrations to stabilize, irradiation was initiated. The temperature (T), relative humidity (RH), and concentrations of O$_3$, NO, and NO$_x$ were continuously monitored. Experiments were run at temperatures ranging 20–26 °C and varied within ±2 °C. RH remained below 10 %. Table 2 summarizes the experimental conditions for the series of methoxyphenol oxidation experiments conducted.

2.2 Gas-phase measurements

2.2.1 Gas chromatography/flame-ionization detection (GC/FID)

The hydrocarbon concentration was continuously monitored by GC/FID in the phenol experiments. Chamber air was sampled into a 10 mL injection loop and injected onto a HP5 15 m × 0.53 mm ID × 1 µm thickness column installed on a 6890 Agilent GC. The GC response was calibrated by dissolving a known mass of the hydrocarbon in methanol and then vaporizing a known volume of that solution into a 55 L Teflon chamber. Guaiacol and syringol measurements obtained using the GC/FID were unreliable due to condensation loss in the sample loop; thus, the hydrocarbon concentration during these experiments was monitored using Chemical Ionization Mass Spectrometry (CIMS) in negative mode operation.

2.2.2 Chemical ionization mass spectrometry (CIMS)

Monitoring of gas-phase oxidation products was carried out in real time by the use of a CIMS instrument. The details of this instrument are described elsewhere (St. Clair et al., 2010). The instrument operates in both negative mode, using CF_3O^- as a reagent ion, and in positive proton transfer reaction (PTR)-MS mode. Negative mode is found to be more selective towards the detection of hydroperoxides and polar molecules, particularly acids, while positive mode detects a broader range of organic compounds. Analytes in negative mode can be monitored as the cluster product $[R \cdot CF_3O]^-$ and/or as the transfer product if it is more strongly acidic $[R \cdot F]^-$, where R is the analyte. Analytes in positive mode cluster as $[R \cdot (H_2O)_n]^+$. Mass scans covering masses 50–300 amu for negative mode, and 50–200 amu for positive mode, with a total scan time of ∼ 6 min were continuously repeated over the course of each experiment. Guaiacol was monitored at the fluoride transfer product ($[M + 19]^-$), m/z 143, and the cluster product ($[M + 85]^-$), m/z 209, in negative mode operation. Syringol was also monitored at the fluoride transfer product, m/z 173, and the cluster product, m/z 239.

2.3 Particle-phase measurements

2.3.1 Chamber filter sample collection, extraction, and off-line chemical characterization

A detailed description of the aerosol filter sample collection and extraction protocol for the Caltech laboratory chambers has been previously published (Surratt et al., 2008). Aerosol samples were collected on Teflon filters (PALL Life Sciences, 47-mm diameter, 1.0-µm pore size, teflomembrane). Filter samplers employed for aerosol filter sample collection used a front and back-up filter sampling approach, in which back-up filters were collected in order to examine if aerosol breakthrough from the front filter occurred or whether evaporation of semivolatiles from the front filter occurred during sampling. In all experiments, no SOA constituents were detected on the back-up filters. Filter sam-

pling was initiated when the aerosol volume reached its maximum (constant) value, as determined by the DMA. Depending on the total volume concentration of aerosol in the chamber, the duration of filter sampling was 1.8–2.1 h, which resulted in 2.0–2.9 m^3 of total chamber air sampled. Teflon filter extraction protocols in high-purity methanol (LC-MS CHROMASOLV-Grade, Sigma-Aldrich) have been described previously (Surratt et al., 2008). The resultant filter extracts were then analyzed by a Waters ACQUITY ultra performance liquid chromatography (UPLC) system, coupled with a Waters LCT Premier TOF mass spectrometer equipped with an ESI source, allowing for accurate mass measurements by UPLC/ESI-TOFMS to be obtained for each ion (Surratt et al., 2008).

Selected filter extracts from experiments were also analyzed by a Thermo Finnigan Surveyor high performance liquid chromatography (HPLC) system (pump and autosampler) coupled to a Thermo Finnigan LCQ ion trap mass spectrometer (ITMS) equipped with an ESI source, allowing for tandem MS measurements to be obtained. Data were acquired and processed using Xcalibur version 1.3 software. A Waters Atlantis T3 column (3 µm particle size; 2.1 × 150 mm) was employed, which is similar to the Water ACQUITY UPLC HSS column used for the UPLC/ESI-TOFMS analysis. The mobile phases consisted of 0.1 % acetic acid in water (A) and 0.1 % acetic acid in methanol (B). The applied 45 min gradient elution program was as follows: the concentration of eluent B was kept at 3 % for 4 min, then increased to 100 % in 21 min, holding at 100 % for 10 min, then decreased to 3 % in 5 min, and kept at 3 % for 5 min. The injection volume and flow rate were 10 µL and 0.2 mL min^{-1}, respectively. The ion trap mass analyzer was operated under the following conditions: sheath gas flow (N_2), 65 arbitrary units; auxiliary gas flow (N_2), 3 arbitrary units; source voltage, −4.5 kV; capillary voltage, −14.5 V; tube lens offset, 7 V; capillary temperature, 200 °C; and maximum ion injection time, 200 ms. Two scan events were used during each chromatographic run; scan event 1 was the full scan mode in which data were collected from m/z 120 to 600 in the negative ionization mode and scan event 2 was the MS2 mode in which product ions were generated from significant base peak ions observed in scan event

1. For MS2 experiments, an isolation width of 2.5 *m/z* units and a normalized collision energy level of 35 % were applied. The $[M-H]^-$ ion signal optimization was carried out by introducing a $1 \, mg \, mL^{-1}$ malic acid standard solution. Due to the on-axis ESI source that is characteristic of the LCQ ITMS instrument, a solvent delay time of 3.5 min (which diverted the column effluent from the ESI source to waste) was employed to prevent clogging by nonvolatile salts at the entrance of the capillary.

2.3.2 High-resolution time-of-flight aerosol mass spectrometry (HR-ToF-AMS)

Real-time aerosol mass spectra were obtained using an Aerodyne HR-ToF-AMS (De-Carlo et al., 2006). The HR-ToF-AMS was operated in a lower resolution, higher sensitivity "V-mode", and a high-resolution "W" mode, switching between modes once every minute. The "V-mode" data were analyzed to extract sulfate, ammonium, and organic spectra according to procedures in Allan et al. (2004). Calculation of the SOA densities were achieved by comparing the particle mass distributions obtained using the particle ToF mode and the volume distributions obtained by the DMA (Bahreini et al., 2005) in nucleation (seed-free) experiments. O:C, N : C, and H : C ratios were determined from "W" mode data using the APES toolbox and applying the procedures outlined in Aiken et al. (2007) and Aiken et al. (2008). The particle-phase signal of CO^+ and the organic contribution to H_xO^+ ions were estimated as described in Aiken et al. (2008).

Particle-into-liquid sampler/ion chromatography (PILS/IC) was also employed as described in Kautzman et al. (2010) for the guaiacol experiments, though we find that $< C_6$ diacids do not constitute an important fraction of the SOA formed.

3 SOA yields and growth curves

The formation of secondary organic aerosol (SOA) results from the gas-particle partitioning of low-vapor-pressure products formed in the oxidation of volatile organic compounds (VOCs). The time-dependent aerosol growth curves permit analysis of the equi-

librium and kinetic roles involved in SOA formation (Chan et al., 2007; Kroll and Seinfeld, 2005). The SOA yield is defined as the ratio of mass of organic aerosol formed, ΔM_o, to the mass of the parent organic species consumed, ΔOrg, $Y = \Delta M_o / \Delta Org$. The SOA yields for all experiments are summarized in Table 2. To calculate the mass concentration of the SOA, the SOA volumes established by DMA measurements are wall-loss corrected and then multiplied by the SOA density, as determined by the AMS in seed-free (nucleation) experiments. A density of $1.65 \, \mu g \, cm^{-3}$ was determined for phenol. Guaiacol and syringol densities were determined to be 1.45 and $1.49 \, \mu g \, cm^{-3}$, respectively. The O:C was calculated at time of maximum SOA growth for these systems and were reported in Chhabra et al. (2011). O:C values of 0.88 ± 0.27, 0.89 ± 0.28, and 0.97 ± 0.30 were calculated for the phenol, guaiacol, and syringol systems, respectively.

About 80 % of the initial phenol was reacted in these experiments. SOA yields for phenol range 25–44 % under the experimental conditions. For phenol, the hydrocarbon measurement obtained from all gas-phase instruments displayed interferences under low-NO_x conditions, leading to a wider spread and greater uncertainty in the yield and growth curve parameters. Still, the measured yields under low-NO_x conditions overlap with the range of 38–45 % reported by Nakao et al. (2011).

Characteristic growth curves for guaiacol are shown in Fig. 1. Greater than 90 % of the initial guaiacol was consumed over the course of all experiments except for the higher guaiacol loading 1/29 experiment as noted in Table 2. SOA yields from guaiacol photooxidation, based on the final aerosol volume achieved, range 44–50 %. Aerosol growth curves under these conditions for all initial guaiacol and seed concentrations fall on a line (Fig. 1), consistent with the formation of essentially non-volatile products.

Aerosol growth curves for syringol are shown in Fig. 2. Within six hours of irradiation, the syringol levels are lower than the limit of detection. The SOA yields for syringol are less than those of guaiacol, ranging 25–37 %. This range overlaps yields of 10–36 % reported for syringol photooxidation under high-NO_x (approaching 10 ppm NO) conducted by Lauraguais et al. (2012) using CH_3ONO as the OH source. The SOA

yields from the photooxidation of syringol are substantially lower than those of phenol and guaiacol, even though the boiling point and vapor pressure of syringol suggest it might have greater potential to form SOA. We further explore the chemical basis for this after examining the gas-phase chemistry.

In this low-NO$_x$ regime, the aerosol growth curves overlap within a system, regardless of initial organic loading. Most methoxyphenol experiments ended shortly after the hydrocarbon decay was complete. Though, even 4 h after 109 ppb syringol was completely reacted in the 3/29 experiment, there was no additional SOA growth. The type of growth observed here is typified by a mechanism involving oxidation to form SOA either from first-generation products or sufficiently rapid low-volatility product formation over the course of the experiment from further generation reactions (Chan et al., 2007; Ng et al., 2006). We believe it to be the latter explanation in the case of methoxyphenol systems. The high-level of oxidation determined from the measured O:C ratios of the SOA are indicative of multi-generation products, which is consistent with the identified gas and aerosol products discussed below.

4 SOA formation chemistry

We present in this section an analysis of the gas-phase mechanistic chemistry involved in SOA formation based on the CIMS traces for each system along with SOA mass growth over time. All ions unless otherwise noted were monitored during negative mode operation. CIMS signals are plotted in arbitrary units (a.u.). Discussion is focused on the guaiacol system since the offline aerosol filter analyses complement the gas-phase data. Chemical parallels are drawn between the three systems.

4.1 Gas-phase oxidation

Substituent groups such as -OH and -OCH$_3$ activate more strongly the aromatic ring towards electrophilic addition of OH compared to the -CH$_3$ group. Of these groups, activa-

tion potential of the ring increases in order of -CH$_3$ < -OCH$_3$ < -OH. Thus, as predicted, methoxyphenol compounds react faster with OH than their methyl or unsubstituted equivalents (Coeur-Tourneur et al., 2010). Methoxy and hydroxy substituent groups tend to make OH-attack favorable at positions *ortho* and *para* to the substituents, so structures for the measured *m/z*'s are proposed from chemical mechanisms assuming one of these positions of initial OH-attack. H-atom abstraction from the methoxy group is expected to be small, as this path was determined to contribute < 4 % in the case of methoxybenzene (Coeur-Tourneur et al., 2010).

A generation is defined as the OH-initiated reaction of a stable (non-radical) species, and the OH exposure is calculated as the product of the OH concentration (inferred from the parent hydrocarbon decay) and the hours of irradiation. Each *m/z* is the sum of the signal from all isomeric structures detected by the CIMS at that ion, but are not shown explicitly in the abbreviated mechanisms and tables presented. However, from the chemical ionization method employed, we expect certain common chemical features of the proposed structures. For example, many of the transfer [M+19]$^-$ products are likely acidic, containing carboxylic acid groups and/or sufficient acidic hydroxyl groups.

4.2 Phenol chemistry

Initial steps of the phenol gas-phase mechanism have been elucidated elsewhere (Olariu et al., 2002; Berndt and Boge, 2003). Phenol + OH proceeds primarily with *ortho*-OH addition to the ring, O$_2$ addition, followed by elimination of HO$_2$ to form 1,2-dihydroxybenzene (catechol). In the low-NO$_x$ phenol experiments, CIMS ions are tracked that show successive OH adduct product formation up to three generations. Quinone products are also likely, though these are not detected in negative mode operation of the current CIMS technique unless they are additionally functionalized. A list of ions monitored in this system is presented in Table 3. Representative data for the phenol low-NO$_x$ system are shown in Fig. 3. Phenol, C$_6$H$_6$O, is monitored at *m/z* 179, a cluster product. We do not include *m/z* 113, the fluoride transfer product, because

this signal includes interference from another compound (likely a small acid) that grows in over time. Dihydroxybenzene, $C_6H_6O_2$, is observed primarily as the fluoride transfer product m/z 129 (DHB) with less signal observed at the m/z 195 cluster product. A trace at m/z 211 indicates a third OH addition to the ring to form trihydroxybenzene (THB), $C_6H_6O_3$. These time profiles are shown along with SOA growth and phenol decay for the first nine hours of irradiation (Fig. 3). SOA growth occurs coincident with the growth of m/z 211 (THB), indicating that the transition to lower volatility products to form SOA likely occurs along the 3rd addition of OH just after $\sim 1 \times 10^6$ molec cm^{-3} h of OH exposure. This is the approximate equivalent of one hour of photooxidation in the atmosphere assuming an ambient OH concentration of $\sim 1 \times 10^6$ molec cm^{-3}. There was very little signal at m/z 227, presumably $C_6H_6O_4$ (4HB) and a minor amount at m/z 229, the hydroperoxide $C_6H_8O_4$.

Figure 3 also shows that the SOA is in equilibrium with m/z 185, which we propose to be the ring fragment $C_4H_4O_3$, a carboxylic acid that forms from the decomposition of the bicyclic radical from phenol + OH. Another carboxylic acid, $C_4H_4O_4$, is monitored at m/z 135, which could be the analogous ring fragment from dihydroxybenzene + OH. These acids approach the high O:C ratios characteristic of the SOA in this system. Comparisons of the CIMS gas-phase traces and the offline filter analyses from similar experiments performed by Nakao et al. (2011) provide additional insights. Nakao et al. (2011) utilized electrospray ionization and atmospheric pressure chemical ionization mass spectrometry (ESI/APCI-TOFMS) as well as PILS-ESI-TOFMS for analysis, though Nakao et al. (2011) noted that the PILS-ESI-TOFMS spectra may include water soluble gas-phase species because a denuder was not used. While Nakao et al. (2011) observed an exact mass match that corresponds with the bicyclic hydroperoxide from phenol ($C_6H_8O_6$) and another compound with a suggested formula $C_6H_8O_7$ using both techniques, we do not observe these products in the gas-phase with the CIMS. It is possible that these compounds are of sufficiently low volatility at this point that they are not measurable in the gas phase. The CIMS does detect ions corresponding to several

$< C_6$ products seen in Nakao et al. (2011), including: $C_4H_4O_3$ at m/z 185, $C_4H_4O_4$ at m/z's 135 and 201, and $C_3H_4O_3$ at m/z 107.

Nakao et al. (2011) also observed a series of oxygen additions, from $C_6H_6O_2$ to $C_6H_6O_5$, which are interpreted to possibly be a series of OH adduct products. Another structural possibility is that these are C_6 retaining, but ring-opened carboxylic acids that would correspond to large signals in the CIMS as transfer products: m/z's 145, 161, and 177. From the time profiles of these CIMS ions, we predict that they are likely carboxylic acids even though the proposed chemical formulae are isomeric to the aromatic OH adducts. The prevalence of these products may explain the absence of a strong signal from a hydroperoxide $C_6H_8O_4$ at m/z 229. The alkylperoxy radical preferentially isomerizes to form the bicyclic peroxide radical and decomposes to $< C_6$ fragments as mentioned above, or it may participate in chemistry that regenerates OH and opens the ring (Birdsall et al., 2010). Figure 4 outlines a potential mechanism similar to that presented in Birdsall et al. (2010) to form these multifunctional C_6 carboxylic acids from phenol, dihydroxybenzene, and trihydroxybenzene. OH regeneration could also come from photolysis of a hydroperoxide producing a favorable alkoxy radical for ring opening, though we would not expect this to be significant on such a quick timescale that is consistent with negligible signal from the hydroperoxide. All CIMS traces for proposed ring opening acids (ACID) and ring fragments (FRAG) are presented in Fig. 5. They all share a similar trend of constant linear growth over time.

4.3 Guaiacol chemistry

Figure 6 presents proposed oxidation pathways for the guaiacol system under low-NO$_x$ conditions. Solid boxed structures indicate that the expected m/z from the chemical ionization reactions in the CIMS for that compound was detected. The m/z monitored is indicated, as are proposed $C_xH_yO_z$ formulas and molecular weights. A list of ions monitored in this system is presented in Table 4. Chemical formulas shown in red indicate correspondence with a suggested $C_xH_yO_z$ for accurate mass observations in filter data (Table 5). The particular structures in Fig. 6 indicate potential structures for

the accurate mass suggested chemical formulae and the mechanism does not explicitly present all potential isomeric structures. The boxed colors correspond with the colors used for ion time traces as measured by the CIMS and included in Fig. 7.

Guaiacol gas-phase oxidation proceeds with OH addition to the ring, followed by reaction with oxygen to form an organic peroxy radical. Under the experimental conditions, the fate of this RO_2 radical is reaction with HO_2 to form a hydroperoxide (Fig. 6, pathway 1), elimination of HO_2 to retain aromaticity (Fig. 6, pathway 2), or isomerization to the bicyclic radical (Fig. 6, pathway 3).

4.3.1 Pathway 1: $RO_2 + HO_2$

Despite predominant conditions of $RO_2 + HO_2$ chemistry, we do not observe strong signals in the CIMS measurements for potential hydroperoxides, as is similar to the case of phenol. A small trace at m/z 259 suggests that there is slight production of the hydroperoxide $C_7H_{10}O_5$. The offline filter analysis does reveal a small contribution from a corresponding accurate mass measurement (Table 5). More significant signals in the CIMS are presented in Fig. 7, demonstrating that the preferred routes are to preserve aromaticity or involve isomerization to the bicyclic radical. This observation is consistent with previous studies on aromatic systems (Calvert et al., 2002; Bloss et al., 2005; Johnson et al., 2005; Birdsall et al., 2010).

4.3.2 Pathway 2: continuous OH addition to ring

The general chemical development of the consecutive OH addition pathways in the guaiacol low-NO_x system are tracked in Fig. 7. Figure 6, pathway 2 is marked by m/z 225 on the CIMS, a cluster product for the guaiacol OH-adduct product, $C_7H_8O_3$ and denoted as G + OH. Successive OH addition products are monitored at 16 amu increments at m/z's 241 and 257, for $C_7H_8O_4$ denoted as G + 2OH and $C_7H_8O_5$ denoted as G + 3OH, respectively. The third OH adduct can be tracked at both the transfer and the cluster products, m/z 191 and m/z 257, respectively. However, m/z 257 includes the

3499

combined signal of rapid epoxide formation and the later formed third generation OH adduct. A signal at m/z 191 is predominantly the third generation OH adduct during the first 8 h until another product (likely an acid) grows in at this m/z. The first OH-adduct product (m/z 225) is short-lived due to further activation of the ring by the additional hydroxy group. Formation of $C_7H_8O_4$ monitored at m/z 241 follows promptly. The signal at m/z 191 (not shown) was observed to follow after m/z 241, indicating that third OH addition is achieved. $C_7H_8O_5$ is also a proposed chemical formula for a product observed in the filter analysis (Table 5), suggesting that the third OH adduct is of sufficiently low volatility to partition to the particle phase.

4.3.3 Pathway 3: isomerization to bicyclic radical

The bicyclic peroxy radical can react with HO_2 to form the bicyclic hydroperoxide $C_7H_{10}O_7$ (Fig. 6, pathway 3ai), however no evidence exists for this product in the CIMS. This is analogous with the bicyclic hydroperoxide from the phenolic case. However, if this product is formed, it already has a low vapor pressure and an O:C of 1, and would likely partition into the aerosol phase. Filter data also indicate the presence of $C_7H_{10}O_7$ in the particle-phase (Table 5). The majority of the filter data guaiacol products exhibit O:C ratio > 0.7, and the average bulk O:C ratio as measured by the AMS is 0.89, so it is likely these hydroperoxide species may immediately partition and become further processed in the particle phase.

Alternatively, the bicyclic radical can rearrange, breaking the oxygen bridge to form an epoxide and open the ring (Fig. 6, pathway 3aii). There is evidence of a significant epoxide (EPOX) route that grows in early with the dihydroxybenzene route (Fig. 7). The epoxide is monitored at m/z 257, the cluster product of $C_7H_8O_5$ (Fig. 7), though there is some later contribution from the third generation OH adduct, as mentioned earlier. The epoxide will continue to react with OH to generate more functionalized molecules that will likely contribute to SOA formation.

The bicyclic radical can also decompose to several fragments as shown in the box in Fig. 6, pathway 3aiii. A major fragment is observed at m/z 149, which could be the

3500

methoxy analog to the phenolic fragment, hydroxy-butenedial ($C_4H_4O_3$) at m/z 185. We propose that m/z 149 is a methoxy-hydroxy-butenedial fragment, $C_5H_6O_4$. $C_5H_6O_4$ is also an accurate mass assignment for a product observed in the filter data (Table 5). The m/z 149 trace has a similar profile to the SOA mass curve, indicating that it is in equilibrium with the particle phase (Fig. 7). Other possible fragments are observed at m/z's indicated in the mechanism. The $< C_4$ fragments approach O:C values > 1, and the C_4 and C_5 fragments would likely undergo further oxidation in the gas phase and then possibly contribute to the particle phase. The fate of butenedial ($C_4H_4O_2$) has been described elsewhere (Calvert et al., 2002; Bloss et al., 2005).

4.3.4 Pathway 4: methoxy loss route

The early growth of a strong signal at m/z 129 (Fig. 7) and a matching time profile at m/z 195 upon irradiation suggests that dihydroxybenzene ($C_6H_6O_2$) is somehow formed from guaiacol ($C_7H_8O_3$) + OH in the gas phase. This is further supported by matching time profiles from the guaiacol and phenol systems for dihydroxybenzene (DHB) and its oxidation to trihydroxybenzene (THB) in Fig. 8a, as well as growth of the proposed C_6 ring opening acids (Fig. 8b). In the guaiacol system, the raw signal at m/z 211 includes contributions from the [18]O natural isotope peak of the guaiacol cluster product and trihydroxybenzene. The signal at m/z 211 has been corrected to reflect only the contribution from trihydroxybenzene (G-THB). There is negligible signal at m/z 227 in the guaiacol system, indicating that the dihydroxybenzene that is formed proceeds only to one more step of oxidation before the carbon along this route is incorporated into pathways besides continuous OH adduct formation. Rather, the carbon likely ends up in production of ring-opened acids as shown in Fig. 8b.

A trace at m/z 243 is present in the guaiacol system, though because there is negligible signal at m/z 227, it is unlikely that this ion is part of the OH adduct series from dihydroxybenzene as $C_6H_6O_5$. Still, an exact mass match for $C_6H_6O_5$ is the fourth highest product (in terms of area counts) of constituents identified in the filter data, and m/z 243 follows the SOA trace indicating that it may be an important contributor to

the particle phase. In the event that radical placement occurs on the carbon containing the methoxy group during formation of the bicyclic radical, carbon loss may occur by removal of a methyl radical. This leads to formation of a C_6 bicyclic ketone product as outlined in pathway 3b of Fig. 6.

4.3.5 Guaiacol aerosol-phase products

The offline filter analysis suggests that there are additional chemical pathways for this system than those inferred from the gas-phase CIMS measurements. The top fifteen ions (by highest peak area) are presented in Table 5 along with measured masses and suggested corresponding chemical formulae. Of the suggested chemical formulae, the O:C ranges from 0.67 to 1.5. The $< C_7$ components are likely ring fragments that have undergone further oxidation to achieve such high O:C compared to those shown in Fig. 6, pathway 3aiii. Of the C_7 retaining products listed in Table 5, all suggested chemical formulae except $C_7H_5O_5$ can be explained by first-generation products along pathways 1, 2, 3ai, and 3aii (Fig. 6) and the analogous pathways in higher generation chemistry from the OH adducts. Similar structures to those proposed here have been observed previously in EI-MS analyses (Justesen, 2001). However, since many corresponding signals are not observed in the CIMS, it is also possible that a number of these highly oxygenated ($> O_5$) species may be formed in the particle phase.

4.4 Syringol chemistry

The chemistry of syringol under low-NO$_x$ conditions leads to rapid formation of a rich diversity of gas-phase products and SOA growth. Whereas at least two generations of OH oxidation of phenol are required to generate SOA, guaiacol and syringol produce SOA in the first generation. This is clear when comparing the SOA mass curves between systems in Figs. 3, 7, and 9. As expected, syringol is more reactive than guaiacol because of its additional methoxy group. Syringol is detected primarily at the transfer [M+19]$^-$, m/z 173, with some signal at the cluster product [M+85]$^-$, m/z 239. This

is the opposite of guaiacol, the signal of which is found predominantly at the cluster product. This suggests that the extra methoxy group on syringol compared to guaiacol leads to an enhancement towards greater acidity to be seen predominantly at the transfer product. This shift is observed for many of the ions in the syringol case that are analogous to the guaiacol system. CIMS ions monitored in this system are presented in Table 6.

Syringol oxidation chemistry seems to undergo similar routes as guaiacol with analogous ions monitored by the CIMS for the following pathways: (1) hydroperoxide formation, (2) OH adduct formation up to two to three generations, and (3) epoxide and $< C_8$ ring fragment formation from decomposition of the bicyclic radical. These pathways are highlighted in Fig. 9a by selected ions at m/z's 189 and 271 for OH adducts $C_8H_{10}O_4$ (S + OH) and $C_8H_{10}O_5$ (S + 2OH), respectively, m/z 287 for the $C_8H_{10}O_6$ syringol epoxide (SEPOX), and a $C_6H_8O_5$ ring fragment (FRAG) at m/z 245. A minor contribution from the $C_8H_{12}O_6$ syringol hydroperoxide at m/z 289 was observed in the CIMS spectra and is not shown.

These routes seem to be minor, however, in comparison to those that favor immediate scission of the C_8 backbone (Fig. 9). Many of the higher signals in the CIMS are at m/z values that can only be reasonably explained by $< C_8$ molecular formulas. For example, major traces are from ions at m/z 275 (Fig. 9b), likely $C_7H_{10}O_6$. A signal was also observed in the CIMS spectra at m/z 291, possibly $C_7H_{10}O_7$, and is not shown. There is also evidence of methoxy and hydroxy exchanges and eliminations, providing even more diversity of masses in the CIMS spectra from syringol photooxidation. More detailed analyses on chemical structure would be required to confirm precise mechanisms.

For syringol, the immediate loss of carbon through novel chemical pathways (methoxy group elimination or exchange with hydroxy) is more evident in multiple routes than was observed in the case of guaiacol. Figure 10 proposes several possibilities of syringol conversion to compounds with fewer methoxy groups. Each of these pathways

3503

has representative ions that also appear in the guaiacol case, though they are not necessarily the same mechanistically.

Analogous to the formation of dihydroxybenzene in the case of guaiacol + OH, the early growth of m/z 225 (presumably $C_7H_8O_3$) suggests that hydroxy guaiacol (G + OH) may form from syringol + OH (Figs. 9b, 10, pathway a). Another possibility is the complete exchange of both methoxy groups for hydroxy groups, resulting in trihydroxybenzene (THB) monitored at m/z 211 (Figs. 9b, 10, pathway b). Formation of guaiacol is also evident by matching time profiles growing in at m/z 143 and 209 (Figs. 9b, 10, pathway c). Growth of dihydroxybenzene (DHB) at m/z 129 and m/z 195 is observed later in the experiment, likely from conversion of guaiacol (Fig. 10, pathway d). Observation of signal at m/z 257 (the guaiacol epoxide and third OH adduct) supports that there is a guaiacol channel in syringol photooxidation, and is not shown. Though a guaiacol channel exists, the coincident formation of m/z 225 (G + OH) and m/z 211 (THB) with that of guaiacol at m/z 209 is consistent with their direct formation from syringol + OH.

4.5 Novel chemical pathways for loss of carbon in methoxyphenol systems

We observe evidence that guaiacol and syringol OH-initiated photooxidation leads to loss of carbon, likely due to unique chemistry involving the methoxy group. While gas-phase aromatic chemistry is not completely understood (Calvert et al., 2002), we propose possible explanations for these novel carbon loss pathways that seem specific to the methoxyphenols. Aihara et al. (1993) studied two pathways in which 1,2-dihydroxybenzene (catechol) forms from o-methoxyphenols using a copper(II)-ascorbic acid-dioxygen system: hydroxyl radical attack ipso to the methoxy containing carbon, and H-abstraction from the methoxy group. Hydroxy radical attack ipso to the methoxy containing carbon allows for loss of the methoxy (-OCH$_3$) group in the form of methanol (CH$_3$OH), removing a C atom from the parent molecule. During H-abstraction from the methoxy group, Aihara et al. (1993) propose that the OCH$_2$ radical reacts with the OH radical and then elimination of formaldehyde (HCHO) ensues. In isotopically labeled

3504

studies, Aihara et al. (1993) observed transformation of guaiacol to catechol and syringol to hydroxy guaiacol. They also measure yields of these products that might imply ipso addition of OH being a more important route than previously considered compared to *ortho*- and *para*-OH addition to the ring. This route could serve as explanation of the observed hydroxy substitutions of methoxy groups in the current systems, but they cannot be verified without measurements of methanol and formaldehyde.

While we see ions indicating that methoxy groups may convert to hydroxyl groups, we do not see evidence supporting the addition of or reversible exchange of methoxy groups to the ring. Methoxy radicals may be formed from photolysis of the $C-OCH_3$ bond, if we assume that this bond energy can be proxied by the bond in dimethylether (CH_3-OCH_3). This bond energy, $351.9\,kJ\,mol^{-1}$ (Luo, 2007), translates to an approximate wavelength of 340 nm, exactly where the irradiance spectrum of the light source in our atmospheric chambers peaks. In the event that methoxy radicals are formed, though, it seems unlikely that methoxy radical reaction with the methoxyphenols results in methoxy addition to the ring or replacement of a hydroxy group, especially compared to rapid reaction with O_2. Gomez et al. (2001) studied the reaction rate constants for methoxy radical with cyclohexane, cyclohexene, and 1,4-cyclohexadiene. It was found that methoxy radical reaction with these compounds is likely to result in preferential H abstraction with minor routes of addition to cyclohexene and 1,4-cyclohexadiene. This corroborates the absence of $>C_7$ species in the guaiacol case and $>C_8$ species in the syringol case.

Thermodynamic evaluation of the substituent group effects in methoxyphenols can also provide some insight. The following discussion is based on the work presented in Varfolomeev et al. (2010) that examines pairwise substitution effects, and inter- and intramolecular hydrogen bonds in methoxyphenols and dimethoxybenzenes. Varfolomeev et al. (2010) show that intramolecular hydrogen bonding plays a significant role on *ortho*-methoxy substituted phenols. This leads to *o*-methoxyphenols having a lower phenolic $O-H$ bond dissociation energy (BDE) compared to *meta* isomers and higher than *para* isomers. This means that the phenolic $O-H$ BDE increases in order

the order 4-methoxyphenol < 2-methoxyphenol < 3-methoxyphenol. From the ab initio calculations of Varfolomeev et al. (2010), the enthalpy of formation for 2-methoxyphenol (guaiacol) is expressed below:

$$\Delta_f H_m^\circ(\text{2-methoxyphenol}) = \Delta_f H_m^\circ(B) + \Delta H(H \rightarrow OH) + \Delta H(H \rightarrow OCH_3)$$
$$+ (ortho-\text{OH-OCH}_3),$$

where $\Delta_f H_m^\circ(B)=$ enthalpy of formation of benzene, $\Delta H(H \rightarrow OH) = -179.0\,kJ\,mol^{-1}$, the increment in enthalpy for substitution of an H atom by -OH, $\Delta H(H \rightarrow OCH_3) = -150.5\,kJ\,mol^{-1}$, the increment in enthalpy for substitution of an H atom by -OCH$_3$, and $(ortho\text{-OH}-OCH_3) = 4.5\,kJ\,mol^{-1}$, the increment in enthalpy for the pairwise interactions of -OH and -OCH$_3$ *ortho* to one another.

The enthalpy of formation expression begins with the base enthalpy of formation from benzene, then adds the effects of hydroxy or methoxy substitution to the ring. Finally, the pairwise interactions are added, reflecting the stabilizing intramolecular H bonding and destabilizing effect from sterics in the *ortho*-OH$-OCH_3$ configuration. From comparison of the substitution effects alone, this suggests that $H \rightarrow OH$ is slightly more favorable than $H \rightarrow OCH_3$. For example, this might support substitution of a methoxy group by a hydroxy group in the guaiacol system, as the pairwise *ortho* effect is minimal.

Assuming that the Varfolomeev et al. (2010) formulation can be extended to the case of a trisubstituted benzene, we can write an analogous expression for the case of syringol (2,6-dimethoxyphenol):

$$\Delta_f H_m^\circ(\text{2,6-dimethoxyphenol}) = \Delta_f H_m^\circ(B) + \Delta H(H \rightarrow OH) + 2 \times \Delta H(H \rightarrow OCH_3)$$
$$+ 2 \times (ortho-\text{OH-OCH}_3) + (meta-\text{OCH}_3\text{-OCH}_3),$$

where $(meta-\text{OCH}_3\text{-OCH}_3)=0.1\,kJ\,mol^{-1}$ from Varfolomeev et al. (2010).

After writing a similar expression for 3-methoxybenzene-1,2-diol (hydroxyguaiacol), the difference between the substituent effects for hydroxyguaiacol and syringol is

$-30\,\text{kJ}\,\text{mol}^{-1}$, in slight favor of hydroxyguaiacol. The pairwise effect of (*ortho*-OH-OH) was not calculated by Varfolomeev et al. (2010), but assuming that it is less sterically hindered compared to (*ortho*-OH-OCH$_3$) and is stabilized by intramolecular hydrogen bonding similar to 1,2-dimethoxybenzene, we assume it to be $< 4.5\,\text{kJ}\,\text{mol}^{-1}$. Due to the combined favorability of energetics for the substituent effects and the pairwise effects, this can help explain why some of the syringol rapidly converts to hydroxyguaiacol and even trihydroxybenzene.

The "phenolic route", involving OH addition at the *ortho* position to the main electron-donating substituent group has been cited as being the main channel responsible for SOA formation in many aromatic systems (Calvert et al., 2002; Johnson et al., 2005; Nakao et al., 2011). However, with the additional methoxy groups, OH attack alpha to the methoxy groups becomes competitive and changes the potential for maintaining aromaticity in the methoxyphenol systems. It is possible that the extra methoxy group in syringol inhibits OH attack that is typically favored *ortho* to the hydroxyl substituted carbon in other systems that generate SOA via this route. For the other compounds, in order to achieve the degree of oxidation of the aerosol, it appears that at least two steps of reaction are needed, but that these steps occur fairly rapidly. If subsequent OH reactions are even slower due to the extra methoxy group in the case of syringol, then conversion to SOA may not be as complete as with the other two compounds over the duration of the experiments reported here.

4.6 Chemical basis for observed yields

The AMS high-resolution spectra for the methoxyphenol systems are distinct. Initial aerosol growth in the guaiacol system is marked by the exact mass ion $C_4H_3O_2^+$. Later the aerosol growth is characterized by the ions $C_2H_3O^+$, and $C_2H_5O_2^+$. In the case of syringol, initial growth is characterized by $C_5H_2O_2^+$ and $C_7H_9O_3^+$ ions, followed by $C_5H_5O_4^+$, and then by $C_5H_2O_4^+$ and $C_2H_4O_3^+$. This suggests that guaiacol SOA is char-

acterized by smaller carbon number and less oxygenated fragments than the case of syringol.

The characteristic ions from the AMS spectra for syringol SOA seem counter-intuitive for understanding why the syringol SOA yield is lower than that of guaiacol. Syringol has more carbon and oxygen to begin with and these ions are larger, more oxygenated fragments than in guaiacol. However, if we return to the gas-phase comparison of the characteristic trends in the guaiacol (Fig. 7) and syringol (Fig. 9) systems, one notes that many of the major products from syringol photooxidation peak later than their analogs in the guaiacol system. Further, there is no analogous peak in the guaiacol system to the *m/z* 275 unique to the syringol system. Since this is a major product of gas-phase syringol photooxidation and it peaks $> 4 \times 10^6\,\text{molec}\,\text{cm}^{-3}\,\text{h}$ of OH exposure compared to guaiacol ions that peak generally within $3 \times 10^6\,\text{molec}\,\text{cm}^{-3}\,\text{h}$, it acts like a gas-phase carbon reservoir. That is, the signal at *m/z* 275 is much more significant than the more efficient SOA formers at *m/z* 129 (dihydroxybenzene, not shown) and *m/z* 209 (guaiacol) in Fig. 9b.

AMS elemental analyses of SOA from these systems as reported in Chhabra et al. (2011) suggest that the majority of oxygenation is derived from organic acid functionalities: 77 % for phenol, 61 % for guaiacol, and 59 % for syringol. This is consistent with the necessity of further oxidation of acidic fragments to explain the presence of highly oxidized species observed in the guaiacol filter analyses. The decrease in oxygenation derived from organic acid functionalities from phenol to the methoxphenol systems may reflect the oxygen reserved in OH adduct and aromatic retaining pathways, especially in the case of syringol (Fig. 10). This may also partially explain why the syringol SOA yield is lower if acid formation drives the SOA growth. At similar OH exposures, the syringol system still has not developed an acid signal that tracks well with the SOA growth, as *m/z* 185 does in the phenol system (Fig. 3) and *m/z* 149 does in the guaiacol system (Fig. 7). The *m/z* 245 fragment lags the SOA growth in the syringol system (Fig. 9a). This could be due to the lack of OH addition to the ring on syringol in critical positions that lead to SOA formation via ring-opening acid formation.

5 Atmospheric relevance

While the current experiments were conducted without the addition of NO_x, the chemistry elucidated under these low-NO_x conditions is expected to be relevant for typical atmospheric conditions. For phenol photooxidation in the presence of NO_x, Olariu et al. (2002) measured yields of 0.8 catechol (1,2-dihydroxybenzene), 0.037 1,4-benzoquinone, and 0.058 2-nitrophenol. However, according to kinetic data and yield comparisons for nitrophenol presented in Berndt and Boge (2003), it is likely that this nitro-product formation can be biased due to sufficiently high NO_2 ($\lesssim 800$ ppb) concentrations. Berndt and Boge (2003) point out that for atmospheric conditions with NO_2 of approximately 20 ppb, it is probable that phenoxy radicals also react with O_3 as well as NO and NO_2. This would result in more minor nitrophenol yields in the atmosphere.

Thus, because OH addition dominates over H abstraction, and subsequent O_2 addition to the OH radical adduct is rapid, it is more likely that in the atmosphere, SOA primarily forms via pathways involving higher-generation OH adducts and their respective routes to oxygenated fragments. This is consistent with the chemistry presented in this work. Though we did not observe appreciable evidence of gas-phase hydroperoxides, they may be rapidly incorporated into the particle phase and contribute to peroxide formation, as postulated by Johnson et al. (2005) and observed by Sato et al. (2007) for the case of toluene photooxidation. Sato et al. (2007) also find similar species in the particle-phase under $[NO]_0 = 0.2$ and 1 ppm, still citing O_2 addition to the OH-aromatic adduct as the major channel contributing to SOA formation.

In the presence of moderate NO_x, we would expect the major gas-phase species to be the same as those presented here, with only a minor contribution from nitrogen-containing products. Still, for the studied compounds, novel routes of reaction of alkylperoxy radicals under these low-NO_x conditions may still result in product distributions expected under higher NO_x conditions. First, the aromatic peroxy radicals in the studied systems may preferentially decompose to regenerate OH via novel $RO_2 + HO_2$ chemistry (Birdsall et al., 2010). This is a possible explanation for the observation of

ring-opened acids in phenol and guaiacol. Second, generation of carbonyls via novel rearrangements of ether peroxy radicals (Orlando and Tyndall, 2012), relevant for guaiacol and syringol, would further make the product distributions less distinct from alkoxy radical pathways expected under high-NO_x chemistry.

These observations warrant caution when conducting experiments in the presence of NO_x for aromatic compounds, as derived aerosol yields may be based on chemistry non-representative of the atmosphere. Klotz et al. (2002) found that at high-NO_x conditions (hundreds of ppb to ppm) one must also start to consider reactions of NO_x with the hydroxy radical adduct. At sufficiently high NO_x concentrations, the gas-phase chemistry can generate higher yields of nitroaromatics as compared to the OH aromatic adduct (Koch et al., 2007; Nishino et al., 2008). Nitroaromatics can serve to enhance aerosol yields if sufficient nitro-containing functionalities are achieved or to act as gas-phase carbon reservoirs and depress aerosol yields. Hydroxyl groups will lead to a vapor pressure lowering more than that associated with nitro groups, but sufficient nitro groups could lead to incorporation to the particle phase. Owing to the lower OH reactivity of the molecule containing a nitro group as compared to the comparable molecule containing a hydroxyl group (Kwok and Atkinson, 1995), one might also find that more OH is necessary in the presence of NO_x to attain further gas-phase development to more highly oxidized species that contribute to SOA formation.

While the OH-initiated photooxidation of aromatics in general is complex (Calvert et al., 2002), methoxyphenols seem to follow some steps of the general mechanism developed for simpler aromatics. We have qualitatively presented gas-phase trends that give some insight into the chemistry of SOA formation. Though, more complete mechanism development would be enhanced by the availability of authentic standards to solidify mass assignments and more detailed structural information. For example, the structural identity of the ion at m/z 275 in the syringol system remains elusive. Calculation of quantitative gas-phase yields would benefit from additional kinetic data pertaining to some of the complex intermediates.

Carbon loss via the methoxy groups in guaiacol and syringol appears to be a feasible route to describe the gas-phase product distributions. While the chemistry of syringol is complex, this compound may be a better model system to represent the mixture of methoxy and phenolic compounds since it displays chemistry from both classes. Syringol, however, does not generate as much SOA as these other systems. This may be a result of the unique OCH_3–OH–OCH_3 pairwise effects that hinder the typical phenolic pathway responsible for SOA formation.

Future studies to investigate this effect might start with methoxyphenols of different substituted positions relative to the hydroxy group to see the effect on SOA yields. For example, using a methoxyphenol where at least one or two methoxy groups are not *ortho* to the hydroxy group would serve to further investigate the importance of OH addition *ortho* to the hydroxy group in these compounds, as 1,2-dihydroxybenzene is the major gas-phase product and SOA fomer from phenol. Also, 2,5-dimethoxyphenol might also indicate if OH attack is preferred at the 6-position, again *ortho* to the hydroxy group. Such studies would require more detailed analyses that provide greater structural analysis for the gas-phase products as well as unique tracers for fragmentation patterns that would clarify the chemistry.

Detailed study of the gas-phase products from the OH-initiated photooxidation of methoxybenzene might also be informative for understanding the proposed carbon loss associated with methoxy groups in the guaiacol and syringol systems. If phenol is a major product, this has implications on understanding the chemical fate of methoxyphenol-like compounds in the atmosphere. For example, Lauraguais et al. (2012) suggest that syringol is too reactive with OH (1.8 h) to be a relevant tracer in the atmosphere for woodsmoke emissions and that it results in a very minor SOA yield. However, the chemical analyses presented in this study suggest that syringol can efficiently convert to guaiacol and hydroxylated benzenes that are longer lived in the atmosphere and potentially have larger SOA yields. This can be analogous to the isoprene photochemical cascade, where it is the products of isoprene photooxidation that have greater SOA forming potential (Kroll et al., 2006). The syringol conversion to guaiacol also has im-

3511

plications for using these compounds as specific tracers for fuel type (hardwood vs. softwood). Thus, care must be taken in selecting one or more surrogate species for use in modeling aerosol yields from biomass burning emissions in the atmosphere.

References

Aihara, K., Urano, Y., Higuchi, T., and Hirobe, M.: Mechanistic studies of selective catechol formation from o-methoxyphenols using a copper(II) ascorbic-acid dioxygen system, J. Chem. Soc. Perk. T., 2, 2165–2170, doi:10.1039/p29930002165, 1993. 3504, 3505

Aiken, A. C., DeCarlo, P. F., and Jimenez, J. L.: Elemental analysis of organic species with electron ionization high-resolution mass spectrometry, Anal. Chem., 79, 8350–8358, 2007. 3493

Aiken, A. C., DeCarlo, P. F., Kroll, J. H., Worsnop, D. R., Huffman, J. A., Docherty, K. S., Ulbrich, I. M., Mohr, C., Kimmel, J. R., Sueper, D., Sun, Y., Zhang, Q., Trimborn, A., Northway, M., Ziemann, P. J., Canagaratna, M. R., Onasch, T. B., Alfarra, M. R., Prevot, A. S. H., Dommen, J., Duplissy, J., Metzger, A., Baltensperger, U., and Jimenez, J. L.: O/C and OM/OC ratios of primary, secondary, and ambient organic aerosols with high-resolution time-of-flight aerosol mass spectrometry, Environ. Sci. Technol., 42, 4478–4485, 2008. 3493

Allan, J. D., Delia, A. E., Coe, H., Bower, K. N., Alfarra, M. R., Jimenez, J. L., Middlebrook, A. M., Drewnick, F., Onasch, T. B., Canagaratna, M. R., Jayne, J. T., and Worsnop, D. R.: A generalised method for the extraction of chemically resolved mass spectra from Aerodyne aerosol mass spectrometer data, J. Aerosol Sci., 35, 909–922, 2004. 3493

Bahreini, R., Keywood, M. D., Ng, N. L., Varutbangkul, V., Gao, S., Flagan, R. C., Seinfeld, J. H., Worsnop, D. R., and Jimenez, J. L.: Measurements of secondary organic aerosol from oxidation of cycloalkenes, terpenes, and m-xylene using an Aerodyne aerosol mass spectrometer, Environ. Sci. Technol., 39, 5674–5688, 2005. 3493

Berndt, T. and Boge, O.: Gas-phase reaction of OH radicals with phenol, Phys. Chem. Chem. Phys., 5, 342–350, doi:10.1039/b208187c, 2003. 3496, 3509

3512

Birdsall, A. W., Andreoni, J. F., and Elrod, M. J.: Investigation of the role of bicyclic peroxy radicals in the oxidation mechanism of toluene, J. Phys. Chem. A, 114, 10655–10663, doi:10.1021/jp105467e, 2010. 3498, 3499, 3509

Bloss, C., Wagner, V., Bonzanini, A., Jenkin, M. E., Wirtz, K., Martin-Reviejo, M., and Pilling, M. J.: Evaluation of detailed aromatic mechanisms (MCMv3 and MCMv3.1) against environmental chamber data, Atmos. Chem. Phys., 5, 623–639, doi:10.5194/acp-5-623-2005, 2005. 3499, 3501

Bond, T. C., Streets, D. G., Yarber, K. F., Nelson, S. M., Woo, J. H., and Klimont, Z.: A technology-based global inventory of black and organic carbon emissions from combustion, J. Geophys. Res.-Atmos., 109, D14203, doi:10.1029/2003JD003697, 2004. 3488

Calvert, J. G., Atkinson, R., Becker, K. H., Kamens, R. M., Seinfeld, J. H., Wallington, T. J., and Yarwood, G.: The Mechanisms of Atmospheric Oxidation of Aromatic Hydrocarbons, Oxford University Press, Inc, New York, USA, 2002. 3499, 3501, 3504, 3507, 3510, 3517

Chan, A. W. H., Kroll, J. H., Ng, N. L., and Seinfeld, J. H.: Kinetic modeling of secondary organic aerosol formation: effects of particle- and gas-phase reactions of semivolatile products, Atmos. Chem. Phys., 7, 4135–4147, doi:10.5194/acp-7-4135-2007, 2007. 3494, 3495

Chhabra, P. S., Ng, N. L., Canagaratna, M. R., Corrigan, A. L., Russell, L. M., Worsnop, D. R., Flagan, R. C., and Seinfeld, J. H.: Elemental composition and oxidation of chamber organic aerosol, Atmos. Chem. Phys., 11, 8827–8845, doi:10.5194/acp-11-8827-2011, 2011. 3494, 3508

Cocker, D. R., Flagan, R. C., and Seinfeld, J. H.: State-of-the-art chamber facility for studying atmospheric aerosol chemistry, Environ. Sci. Technol., 35, 2594–2601, 2001. 3489

Coeur-Tourneur, C., Cassez, A., and Wenger, J. C.: Rate coefficients for the gas-phase reaction of hydroxyl radicals with 2-Methoxyphenol (guaiacol) and related compounds, J. Phys. Chem. A, 114, 11645–11650, doi:10.1021/jp1071023, 2010. 3496, 3517

DeCarlo, P. F., Kimmel, J. R., Trimborn, A., Northway, M. J., Jayne, J. T., Aiken, A. C., Gonin, M., Fuhrer, K., Horvath, T., Docherty, K. S., Worsnop, D. R., and Jimenez, J. L.: Field-deployable, high-resolution, time-of-flight aerosol mass spectrometer, Anal. Chem., 78, 8281–8289, 2006. 3493

Dills, R. L., Zhu, X. Q., and Kalman, D. A.: Measurement of urinary methoxyphenols and their use for biological monitoring of wood smoke exposure, Environ. Res., 85, 145–158, 2001. 3488

Fine, P. M., Cass, G. R., and Simoneit, B. R. T.: Chemical characterization of fine particle emissions from fireplace combustion of woods grown in the northeastern United States, Environ. Sci. Technol., 35, 2665–2675, 2001. 3488

Gomez, N., Henon, E., Bohr, F., and Devolder, P.: Rate constants for the reactions of CH_3O with cyclohexane, cyclohexene, and 1,4-cyclohexadiene: Variable temperature experiments and theoretical comparison of addition and H-abstraction channels, J. Phys. Chem. A, 105, 11204–11211, doi:10.1021/jp010204h, 2001. 3505

Hawthorne, S. B., Krieger, M. S., Miller, D. J., and Mathiason, M. B.: Collection and quantitation of methoxylated phenol tracers for atmospheric-pollution from residential wood stoves, Environ. Sci. Technol., 23, 470–475, 1989. 3488

Hawthorne, S. B., Miller, D. J., Langenfeld, J. J., and Krieger, M. S.: PM-10 high-volume collection and quantification of semivolatile and nonvolatile phenols, methoxylated phenols, alkanes, and polycyclic aromatic-hydrocarbons from winter urban air and their relationship to wood smoke emmisions, Environ. Sci. Technol., 26, 2251–2262, 1992. 3488

Ito, A. and Penner, J. E.: Historical emissions of carbonaceous aerosols from biomass and fossil fuel burning for the period 1870–2000, Global Biogeochem. Cy., 19, GB2028, doi:10.1029/2004GB002474, 2005. 3488

Johnson, D., Jenkin, M., Wirtz, K., and Martin-Reviejo, M.: Simulating the formation of secondary organic aerosol from the photooxidation of aromatic hydrocarbons, Environ. Chem., 2, 35–48, doi:10.1071/EN04079, 2005. 3499, 3507, 3509

Justesen, U.: Collision-induced fragmentation of deprotonated methoxylated flavonoids, obtained by electrospray ionization mass spectrometry, J. Mass Spectrom., 36, 169–178, doi:10.1002/jms.118, 2001. 3502

Kautzman, K. E., Surratt, J. D., Chan, M. N., Chan, A. W. H., Hersey, S. P., Chhabra, P. S., Dalleska, N. F., Wennberg, P. O., Flagan, R. C., and Seinfeld, J. H.: Chemical composition of gas- and aerosol-phase products from the photooxidation of naphthalene, J. Phys. Chem. A, 114, 913–934, 2010. 3493

Keywood, M. D., Varutbangkul, V., Bahreini, R., Flagan, R. C., and Seinfeld, J. H.: Secondary organic aerosol formation from the ozonolysis of cycloalkenes and related compounds, Environ. Sci. Technol., 38, 4157–4164, 2004. 3489

Klotz, B., Volkamer, R., Hurley, M., Andersen, M., Nielsen, O., Barnes, I., Imamura, T., Wirtz, K., Becker, K., Platt, U., Wallington, T., and Washida, N.: OH-initiated oxidation of benzene –
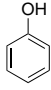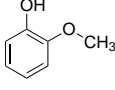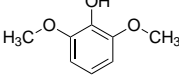
Part II. influence of elevated NO_x concentrations, Phys. Chem. Chem. Phys., 4, 4399–4411, doi:10.1039/b204398j, 2002. 3510

Koch, R., Knispel, R., Elend, M., Siese, M., and Zetzsch, C.: Consecutive reactions of aromatic-OH adducts with NO, NO_2 and O_2: benzene, naphthalene, toluene, m- and p-xylene, hexamethylbenzene, phenol, m-cresol and aniline, Atmos. Chem. Phys., 7, 2057–2071, doi:10.5194/acp-7-2057-2007, 2007. 3510

Kroll, J. H. and Seinfeld, J. H.: Representation of secondary organic aerosol laboratory chamber data for the interpretation of mechanisms of particle growth, Environ. Sci. Technol., 39, 4159–4165, 2005. 3494

Kroll, J. H., Ng, N. L., Murphy, S. M., Flagan, R. C., and Seinfeld, J. H.: Secondary organic aerosol formation from isoprene photooxidation, Environ. Sci. Technol., 40, 1869–1877, doi:10.1021/es0524301, 2006. 3511

Kwok, E. S. and Atkinson, R.: Estimation of hydroxyl radical reaction rate constants for gas-phase organic compounds using a structure-reactivity relationship: an update, Atmos. Environ., 29, 1685–1695, doi:10.1016/1352-2310(95)00069-B, 1995. 3510

Lauraguais, A., Coeur-Tourneur, C., Cassez, A., and Seydi, A.: Rate constant and secondary organic aerosol yields for the gas-phase reaction of hydroxyl radicals with syringol (2,6-dimethoxyphenol), Atmos. Environ., 55, 43–48, doi:10.1016/j.atmosenv.2012.02.027, 2012. 3494, 3511, 3517

Luo, Y. R.: Comprehensive Handbook of Chemical Bond Energies, CRC Press, Boca Raton, FL, 2007. 3505

Naeher, L. P., Brauer, M., Lipsett, M., Zelikoff, J. T., Simpson, C. D., Koenig, J. Q., and Smith, K. R.: Woodsmoke health effects: a review, Inhal. Toxicol., 19, 67–106, 2007. 3488

Nakao, S., Clark, C., Tang, P., Sato, K., and Cocker III, D.: Secondary organic aerosol formation from phenolic compounds in the absence of NO_x, Atmos. Chem. Phys., 11, 10649–10660, doi:10.5194/acp-11-10649-2011, 2011. 3494, 3497, 3498, 3507

Ng, N. L., Kroll, J. H., Keywood, M. D., Bahreini, R., Varutbangkul, V., Flagan, R. C., Seinfeld, J. H., Lee, A., and Goldstein, A. H.: Contribution of first- versus second-generation products to secondary organic aerosols formed in the oxidation of biogenic hydrocarbons, Environ. Sci. Technol., 40, 2283–2297, 2006. 3495

Nishino, N., Atkinson, R., and Arey, J.: Formation of nitro products from the gas-phase OH radical-initiated reactions of toluene, naphthalene, and biphenyl: effect of NO_2 concentration, Environ. Sci. Technol., 42, 9203–9209, doi:10.1021/es802046m, 2008. 3510

Olariu, R. I., Klotz, B., Barnes, I., Becker, K. H., and Mocanu, R.: FTIR study of the ring-retaining products from the reaction of OH radicals with phenol, o-, m-, and p-cresol, Atmos. Environ., 36, 3685–3697, 2002. 3496, 3509

Orlando, J. J. and Tyndall, G. S.: Laboratory studies of organic peroxy radical chemistry: an overview with emphasis on recent issues of atmospheric significance, Chem. Soc. Rev., 41, 6294–6317, doi:10.1039/c2cs35166h, 2012. 3510

Pye, H. O. T. and Seinfeld, J. H.: A global perspective on aerosol from low-volatility organic compounds, Atmos. Chem. Phys., 10, 4377–4401, doi:10.5194/acp-10-4377-2010, 2010. 3487

Sato, K., Hatakeyama, S., and Imamura, T.: Secondary organic aerosol formation during the photooxidation of toluene: NO_x dependence of chemical composition, J. Phys. Chem. A, 111, 9796–9808, doi:10.1021/jp071419f, 2007. 3509

Schauer, J. J., Kleeman, M. J., Cass, G. R., and Simoneit, B. R. T.: Measurement of emissions from air pollution sources. 3. C-1-C-29 organic compounds from fireplace combustion of wood, Environ. Sci. Technol., 35, 1716–1728, 2001. 3488

Simpson, C. D. and Naeher, L. P.: Biological monitoring of wood-smoke exposure, Inhal. Toxicol., 22, 99–103, 2010. 3488

St. Clair, J. M., McCabe, D. C., Crounse, J. D., Steiner, U., and Wennberg, P. O.: Chemical ionization tandem mass spectrometer for the in situ measurement of methyl hydrogen peroxide, Rev. Sci. Instrum., 81, 94–102, 2010. 3491

Surratt, J. D., Gómez-González, Y., Chan, A. W. H., Vermeylen, R., Shahgholi, M., Kleindienst, T. E., Edney, E. O., Offenberg, J. H., Lewandowski, M., Jaoui, M., Maenhaut, W., Claeys, M., Flagan, R. C., and Seinfeld, J. H.: Organosulfate formation in biogenic secondary organic aerosol, J. Phys. Chem. A, 112, 8345–8378, 2008. 3491, 3492

Varfolomeev, M. A., Abaidullina, D. I., Solomonov, B. N., Verevkin, S. P., and Emel'yanenko, V. N.: Pairwise substitution effects, inter- and intramolecular hydrogen bonds in methoxyphenols and dimethoxybenzenes. thermochemistry, calorimetry, and first-principles calculations, J. Phys. Chem. B, 114, 16503–16516, doi:10.1021/jp108459r, 2010. 3505, 3506, 3507

Table 1. Chemical properties.

Compound	Structure	Boiling Pt. (°C)	V.P. @ 25°C (mm Hg)	$k_{OH} \times 10^{-11}$ (molec cm^{-3} s^{-1})
Phenol		182	0.351	2.7 ± 0.25 at 25°C, Calvert et al. (2002)
Guaiacol		205	0.13	7.53 ± 0.41 at 21 ± 2°C, Coeur-Tourneur et al. (2010)
Syringol		260	0.0062	9.66 ± 1.11 at 21 ± 2°C, Lauraguais et al. (2012)
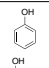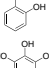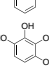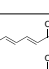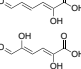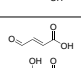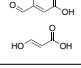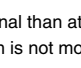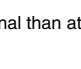
Table 2. Experimental conditions.

Date (2010)	Organic	[Org]$_0$ (ppb)	[Org]$_f$ (ppb)	[NO$_2$]$_0$ (ppb)	[NO]$_0$ (ppb)	V_0 μm^3 cm^{-3}	V_f μm^3 cm^{-3}	Yield
29 Jan	guaiacol	66.3	13.4	< LDL[*]	< LDL[*]	18.2	120.0	0.49
2 Feb	guaiacol	5.9	< LDL[*]	< LDL[*]	< LDL[*]	16.4	25.0	0.46
4 Feb	guaiacol	12.4	< LDL[*]	< LDL[*]	< LDL[*]	13.6	31.0	0.44
6 Feb	guaiacol	45.5	4.1	< LDL[*]	5	12.9	85.0	0.50
11 Feb	phenol	47.6	9.9	< LDL[*]	6	16.0	58.0	0.44
15 Feb	phenol	10.0	2.1	< LDL[*]	5	11.4	20.0	0.40
17 Feb	phenol	73.9	14.4	< LDL[*]	< LDL[*]	12.0	44.0	0.25
20 Feb	phenol	101.9	18.8	< LDL[*]	5	10.0	69.0	0.24
10 Mar	syringol	185.1	< LDL[*]	7	< LDL[*]	11.0	325.0	0.37
15 Mar	syringol	49.5	< LDL[*]	< LDL[*]	< LDL[*]	14.2	67.0	0.25
29 Mar	syringol	112.9	< LDL[*]	9	< LDL[*]	11.7	174.0	0.34

[*] Below lower detection limit.

Table 3. Proposed structures for CIMS ions in the phenol low-NO_x system. C and T indicate the cluster and transfer product, respectively.

Observed m/z	Product	Chemical Formula	Proposed Structure (one isomer shown)	Chemical Pathway
179	C	C_6H_6O		phenol
129	T[a]	$C_6H_6O_2$		DHB = phenol + OH
211	C	$C_6H_6O_3$		THB = DHB + OH
227	C	$C_6H_6O_4$		4HB = THB + OH
145	T	$C_6H_6O_3$		ring opening acid
161	T	$C_6H_6O_4$		ring opening acid
177	T	$C_6H_6O_5$		ring opening acid
185	C[b]	$C_4H_4O_3$		ring fragment
135	T[c]	$C_4H_4O_4$		ring fragment
107	T	$C_3H_4O_3$		ring fragment
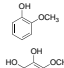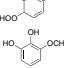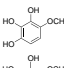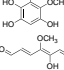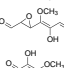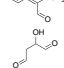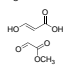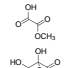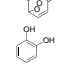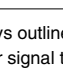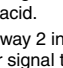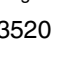
[a] m/z 195 is also present as $C_6H_6O_2$, but is lower signal than at m/z 129.
[b] The transfer product at $C_4H_4O_3$ is at m/z 119, which is not monitored in low-NO_x conditions because it is the cluster product of H_2O_2.
[c] m/z 201 is also present as $C_4H_4O_4$, but is lower signal than at m/z 135.

Table 4. Proposed structures for CIMS ions in the guaiacol low-NO_x system. C and T indicate the cluster and transfer product, respectively.

Observed m/z	Product	Chemical Formula	Proposed Structure (one isomer shown)	Chemical Pathway[a]
209	C[b]	$C_7H_8O_2$		guaiacol
259	C	$C_7H_{10}O_5$		(1) hydroperoxide
225	C	$C_7H_8O_3$		(2) G + OH = guaiacol + OH
241	C	$C_7H_8O_4$		(2) G + 2OH = guaiacol + 2OH
191	T[c]	$C_7H_8O_5$		(2) G + 3OH = guaiacol + 3OH
175	T	$C_7H_8O_4$		ring opening acid
257	C[d]	$C_7H_8O_5$		(3aii) EPOX and (2) G + 3OH
149	T	$C_5H_6O_4$		(3aiii) ring fragment
187	C	$C_4H_6O_3$		(3aiii) ring fragment
199	C	$C_3H_4O_3$		(3aiii) ring fragment
107	T	$C_3H_4O_3$		(3aiii) ring fragment
189	C	$C_3H_4O_4$		(3aiii) ring fragment
243	T	$C_6H_6O_5$		(3b) C_6 bicyclic ketone
129	T[e]	$C_6H_6O_2$		(4) methoxy loss

[a] Numbers indicate correspondence with pathways outlined in mechanism (Fig. 6).
[b] m/z 143 is also present as $C_7H_8O_2$, but is lower signal than at m/z 209.
[c] Also includes signal from $C_7H_8O_5$ ring opening acid.
[d] Includes contributions from G + 3OH along pathway 2 in Fig. 6
[e] m/z 195 is also present as $C_6H_6O_2$, but is lower signal than at m/z 129.

Table 5. SOA products observed in UPLC/(-)ESI-TOFMS offline filter analysis for the guaiacol low-NO_x system.

$[M-H]^-$	Meas. Mass	Suggested Chemical Formula (M)	Error[*] (mDa)
189	189.0378	$C_7H_{10}O_6$	−2.1
219	219.014	$C_7H_8O_8$	−0.1
147	147.0266	$C_5H_8O_5$	−2.6
157	157.0113	$C_6H_6O_5$	−2.4
133	133.0133	$C_4H_6O_5$	−2.4
149	149.0072	$C_4H_6O_6$	−1.4
205	205.0327	$C_7H_{10}O_7$	2.1
145	145.048	$C_6H_{10}O_4$	−2.1
163	163.0233	$C_5H_8O_6$	−1
203	203.0177	$C_7H_8O_7$	−1.5
171	171.0279	$C_7H_8O_5$	−1.4
169	169.0124	$C_7H_6O_5$	−1.3
173	173.0428	$C_7H_{10}O_5$	−2.2
115	115.0004	$C_4H_4O_4$	−2.7
129	129.0175	$C_5H_6O_4$	−1.3

[*] The error in the accurate mass measurements is the difference between the theoretical mass of the suggested molecular formulae of the parent molecule (M) and the measured mass of the ion.

Table 6. Proposed structures for CIMS ions in the syringol low-NO_x system. C and T indicate the cluster and transfer product, respectively.

Observed m/z	Product	Chemical Formula	Proposed Structure (one isomer shown)	Chemical Pathway[a]
173	T[b]	$C_8H_{10}O_3$		syringol
189	T	$C_8H_{10}O_4$		S + OH = syringol + OH
271	C	$C_8H_{10}O_5$		S + 2OH = syringol + 2OH
289	C	$C_8H_{12}O_6$		hydroperoxide
225	C	$C_7H_8O_3$		(a) G + OH = guaiacol + OH
211	C	$C_6H_6O_3$		(b) THB = DHB + OH
209	C	$C_7H_8O_2$		(c) guaiacol
129	T[c]	$C_6H_6O_2$		(d) DHB = phenol + OH
205	T[d]	$C_8H_{10}O_5$		ring opening acid
287	C	$C_8H_{10}O_6$		SEPOX
245	C	$C_6H_8O_5$		ring fragment
149	T	$C_5H_6O_4$		ring fragment
185	C	$C_4H_4O_3$		ring fragment
203	C	$C_4H_6O_4$		ring fragment
275	C	$C_7H_{10}O_6$	none proposed	C_8 scission
291	C	$C_7H_{10}O_7$	none proposed	C_8 scission

[a] Letters indicate correspondence with pathways outlined in mechanism (Fig. 10).
[b] m/z 239 is also present as $C_8H_{10}O_3$, but is lower signal than at m/z 173.
[c] m/z 195 is also present as $C_6H_6O_2$, but is lower signal than at m/z 129.
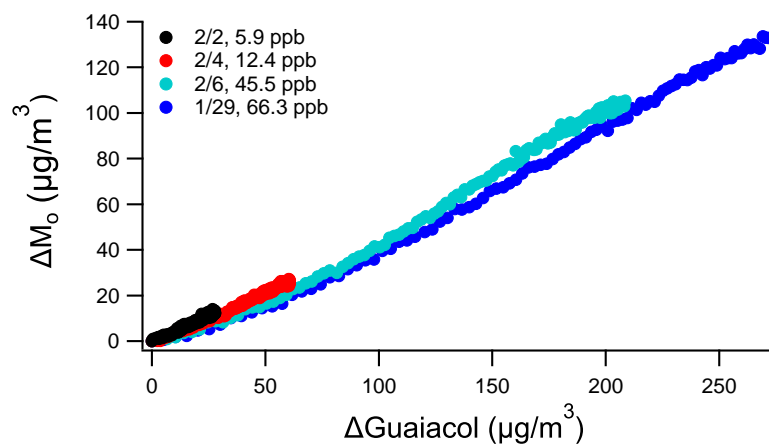[d] Includes contributions from S + 2OH as well as ring opening acid.

Fig. 1. Growth curves of guaiacol aerosol.

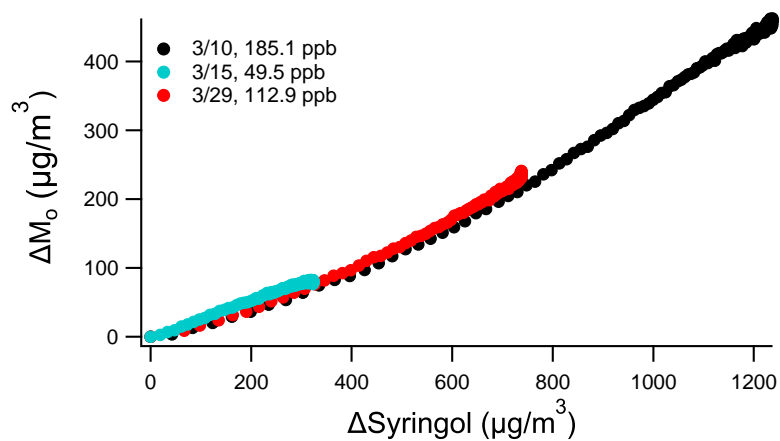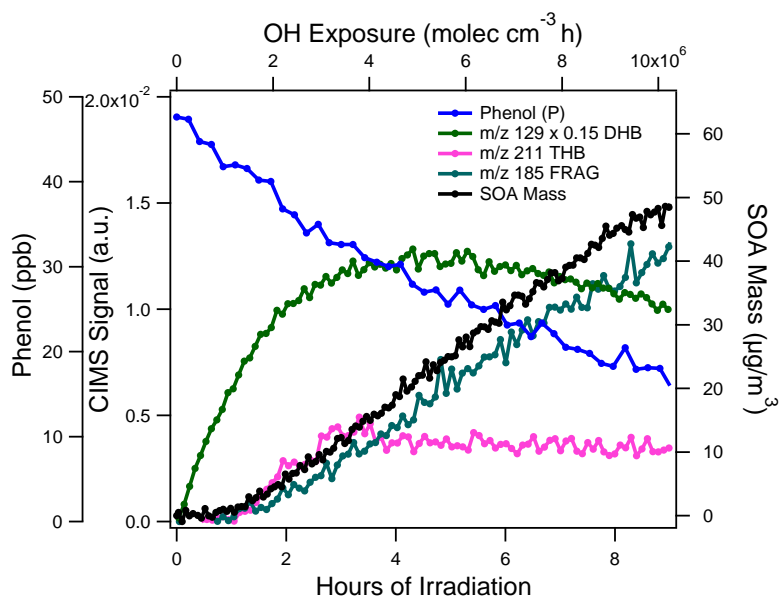**Fig. 2.** Growth curves of syringol aerosol.

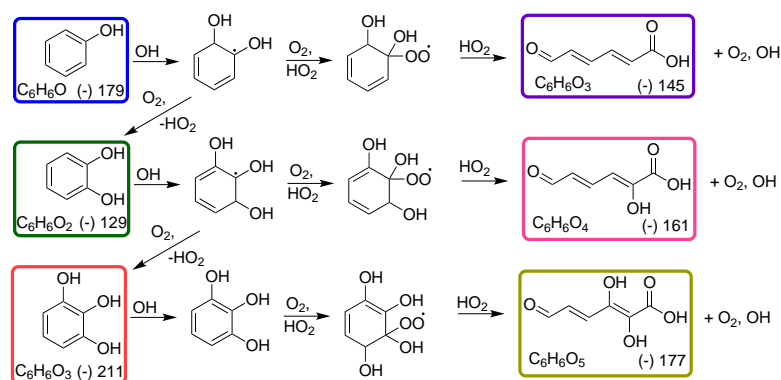**Fig. 3.** Phenol low-NO$_x$ gas-phase and particle-phase development.

Fig. 4. Proposed pathway for gas-phase production of C$_6$ carboxylic acids in the phenol low-NO$_x$ system. Boxed structures indicate that the expected *m/z* from the chemical ionization reactions in the CIMS for that compound was detected.
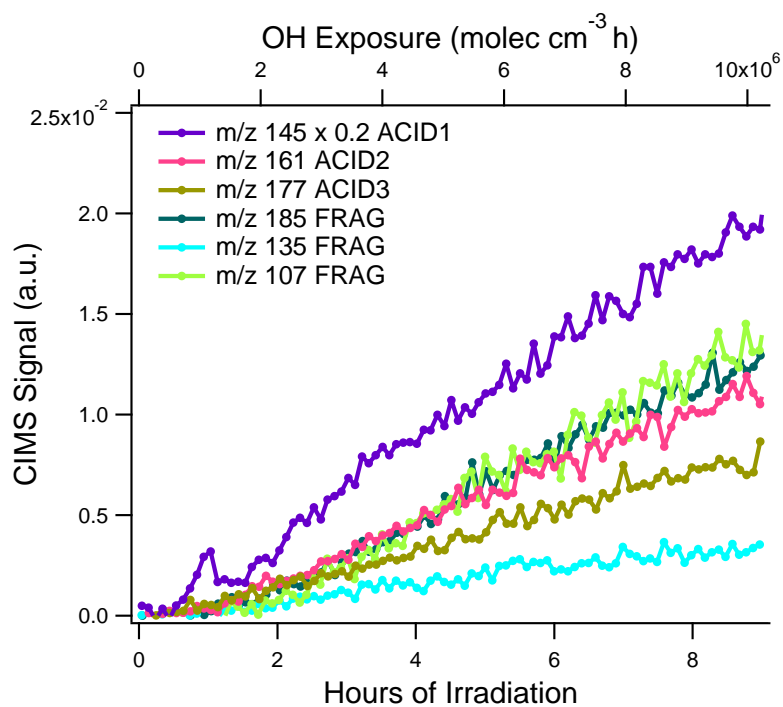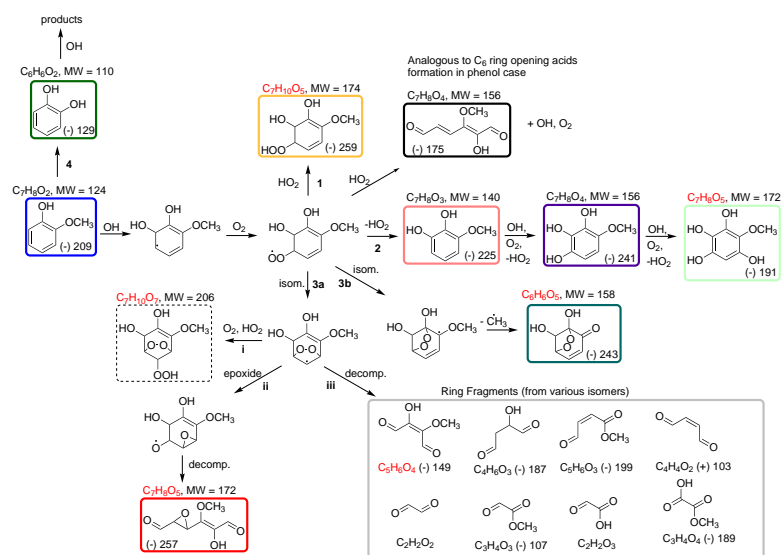
Fig. 5. Selected phenol low-NO$_x$ gas-phase acids.

Fig. 6. Proposed mechanism for guaiacol low-NO$_x$ oxidation. Boxed structures indicate that the expected *m/z* from the chemical ionization reactions in the CIMS for that compound was detected. Chemical formulae in red correspond with those proposed for the filter accurate mass aerosol measurements.
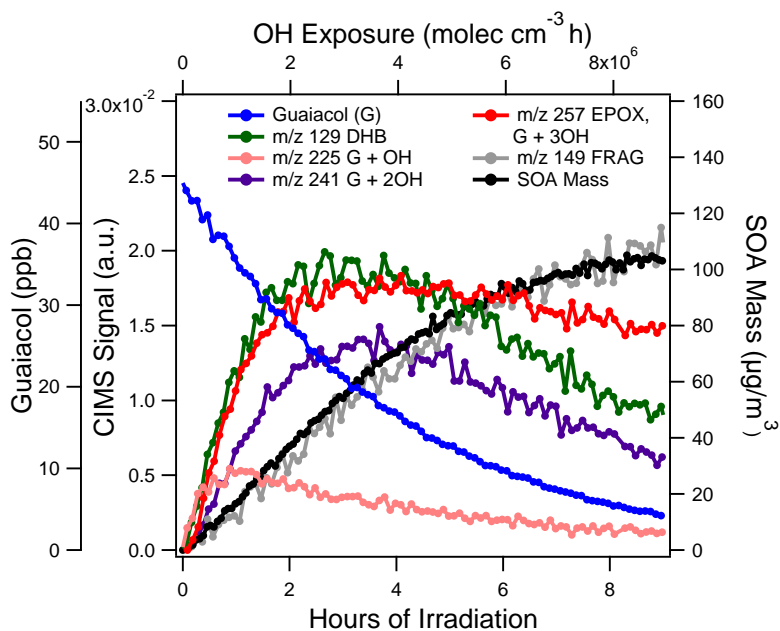
Fig. 7. Selected traces in guaiacol low-NO$_x$ gas-phase and particle-phase development.
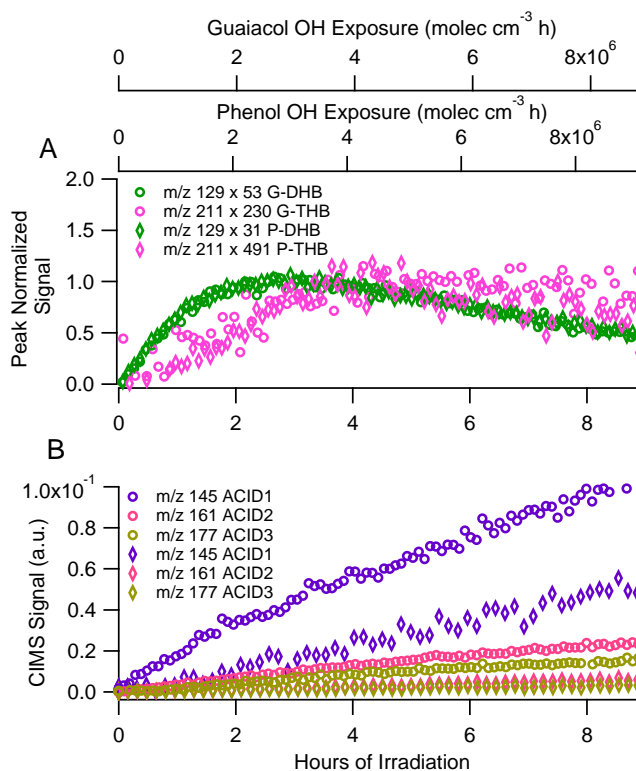
Fig. 8. Common chemical routes in the phenol and guaiacol low-NO$_x$ systems. **(A)** Dihydroxy-benzene routes in phenol (diamonds) and guaiacol (open circles). Each CIMS trace is normalized by the peak value. **(B)** Common acids in phenol (diamonds) and guaiacol (open circles).
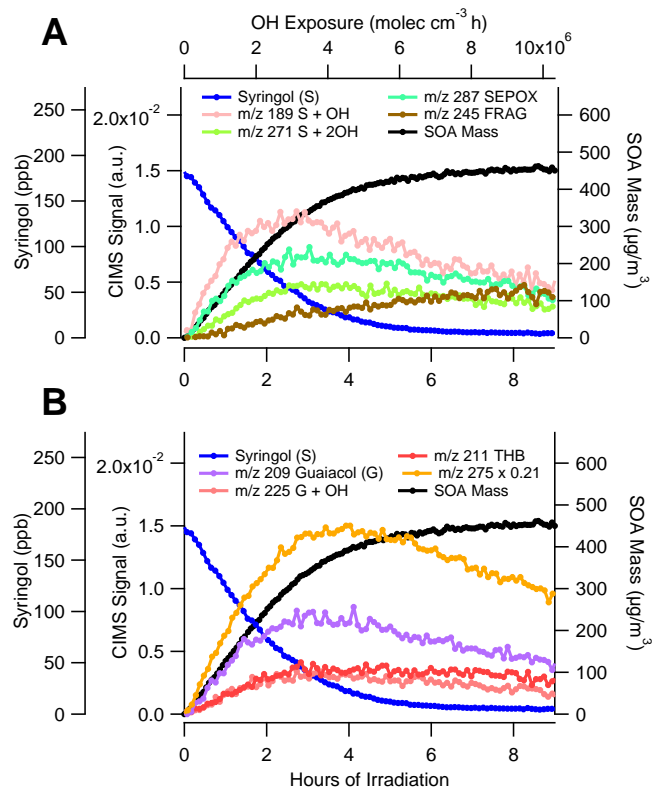
Fig. 9. Selected traces in syringol low-NO$_x$ gas-phase and particle-phase development. **(A)** OH addition pathways. **(B)** Traces indicating methoxy loss pathways.
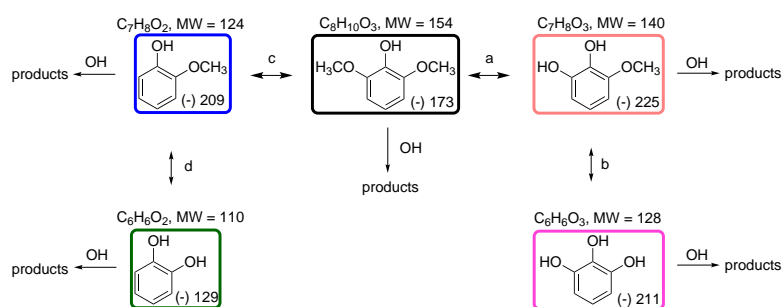
3531

Fig. 10. Possible routes of methoxy loss in syringol gas-phase chemistry.